Universität Stuttgart

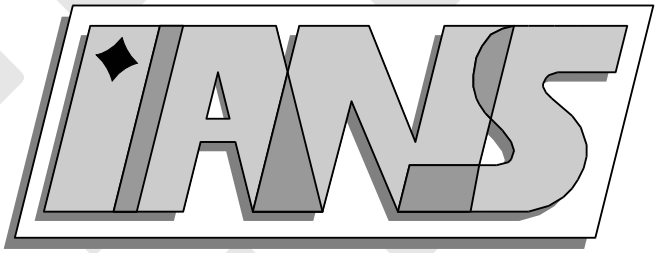

Overlapping domain decomposition for incremental sheet metal forming

Stephan Brunßen, Evgeny Savenkov, Barbara Wohlmuth

Berichte aus dem Institut für Angewandte Analysis und Numerische Simulation

Documentation 2009/014

Universität Stuttgart

Overlapping domain decomposition for incremental sheet metal forming

Stephan Brunßen, Evgeny Savenkov, Barbara Wohlmuth

Berichte aus dem Institut für Angewandte Analysis und Numerische Simulation

Documentation 2009/014

Institut für Angewandte Analysis und Numerische Simulation (IANS)
Fakultät Mathematik und Physik
Fachbereich Mathematik
Pfaffenwaldring 57
D-70 569 Stuttgart

E-Mail: ians-preprints@mathematik.uni-stuttgart.de
WWW: http://preprints.ians.uni-stuttgart.de

ISSN **1611-4176**

1 Introduction

In this work, the results of the research activities within the subproject "Entwicklung effizienter numerischer Simulationsalgorithmen für CNC-gesteuerte inkrementelle Umformverfahren" of the DFG priority program SPP 1146 "Modellierung inkrementeller Umformverfahren" are presented. The main purpose of the research is the construction of efficient numerical algorithms for the incremental metal forming process. The presented results as well as some generalizations have been published in [12, 25, 8, 10, 11, 9, 24, 13] and the thesis [7]. We refer the reader to these papers for more detailed considerations.

Metal forming application To motivate the research work on the subject and present the main challenges of the implicit FE simulation and solution methods we briefly describe two examples for incremental forming processes, namely, the deep-rolling process and the incremental sheet metal forming process.

For a more detailed description of the deep-rolling process and its technical applications, we refer to [30] and the references cited therein. An example of an engineering problem where the application of the deep-rolling process can be efficient is given by the weakening of a turbine blade (see Fig. 1, left). The design of such deep-rolling processes is associated with time- and cost-intensive experiments. Thus, a finite element analysis is very helpful for understanding the complex deformation mechanisms occurring during the rolling contact.

Another important application is incremental sheet metal forming (ISF) which is a recently introduced forming technique [15, 35, 27] (Fig. 1, right). The ISF process is very difficult to control, since wrinkles or even cracks can occur if the computer numerical controlled (CNC) path is not appropriate, and numerical simulation is very useful for the development of optimal forming strategies.

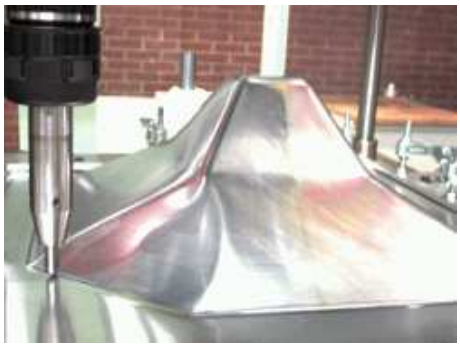

Figure 1: Deep-rolling process (©WZL, Aachen) and incremetal sheet forming (©IBF, Aachen).

Overview of numerical approaches Both applications described above share similar difficulties with respect to their numerical simulation. The most important among them are: (i) The forming zone is small but very mobile, leading to very fine computational meshes and extensive adaptive re-meshing. (ii) Both *physical* and *contact* nonlinearities have to be modeled. These features lead to a lack of efficiency when standard algorithms are applied, and, therefore, new solution techniques have been developed to overcome these difficulties efficiently.

These proposed algorithms are based on the efficient combination of several numerical approaches. Among them, the most important are mortar coupling based on dual Lagrange multipliers and semi-smooth inexact Newton methods. These techniques are well established and have proven their efficiency and robustness in a number of different applications. In this work, we demonstrate how they can be combined in order to provide practical solution techniques fitted for the above mentioned applications.

To handle the nonlinearity of the contact conditions, several methods can be found in the literature. Among them there are penalty formulations as well as standard or augmented Lagrange multipliers approaches.

A great number of contact algorithms developed in the past enforce the contact constraints at specific collocation points. Using a node-to-segment approach, the main idea is that a specific node on the slave side must not penetrate the opposing segment on the master side. Although this approach is quite popular and used in numerous commercial finite element codes, the robustness of these methods is still a limitation in certain applications. Simle forms of these algorithms do not satisfy the contact patch test [37]. Their more coplex versions [38, 36, 44], generally, pass the contact patch test but suffer from locking. Due to these drawbacks, the research on segment-to-segment coupling strategies has become quite active in recent years. Most of these new approaches use the so-called mortar method, initially introduced as a domain decomposition method by Bernardi and co-workers [6]. The reader is referred to [4, 2, 5, 48, 39, 40, 34, 19] and the references therein for an overview of the mortar method in the context of contact problems. Other approaches like penalty methods, are not variationally consistent. Furthermore, large values of the penalty parameter can spoil condition number of the linear sytem to be solved. We refer to [7] for a short overview of the mentioned approaches.

In this work, we use Lagrange multipliers to handle the contact constraints. This approach is variationally consistent, provides exact fulfillment of the discrete contact conditions and does not deteriorate the condition number of the problem. However, one has to take care about the follwoing two important points. First, the finite dimensional space for the dual variables has to be chosen with care in order to satisfy the so-called inf-sup condition. Second, the system of the finite-dimensional equations can have different size during the iterations. The last point can be avoided by using the so-called dual Lagrange multipliers, chosen to be biorthogonal relatively to the standard basis functions. This choice not only provides an inf-sup stable pair of spaces but also lead to diagonal coupling matrices, such that the additional unknowns cab easily be eliminated. The dual Lagrange multipliers have originally been introduced in [45] and have already been applied to problems involving frictional or thermo-mechanical contact [46, 29].

To incorporate the contact conditions, we use nonlinear complementarity functions to rewrite the contact inequality constraints as equalities. This allows to consider both contact and plasticity nonlinearities in a unified way by applying the semi-smooth Newton method to the derived system of nonlinear equations. The result can be interpreted as the primal-dual active set strategy for contact and the radial return method for the plasticity flow rule. This not only leads to an efficient iterative scheme but also allows to consider different regularization techniques to improve the robustness and convergence properties of the Newton method as well as to avoid oversolving effects [22].

Overlapping domain decomposition Due to the local character of the metal forming process, a suitable numerical scheme has to provide a good resolution of the behavior of the forming process in the neighborhood of the working tool. Using classical adaptive approaches, frequent re-meshing is needed, which is a very time-consuming procedure. To avoid this difficulty, we employ a dynamic overlapping domain decomposition method (ODDM) which naturally accounts for the local nature of the contact and plasticity effects.

The complete domain is approximated using a relatively coarse global mesh, whereas a moving local fine mesh is used to resolve the plastification and the contact interaction in the neighborhood of the working tool, providing a suitable correction to the global coarse solution, see Fig. 2 (right).

Of course, the two FE domains have to interchange certain information, mainly the plastic history data and the contact traction. To deal with the former, we split the strain tensor into its elastic and its plastic part and perform the plastic computation only on the fine grid. Similarly, the contact computations are restricted to the fine grid, and the contact stresses are transferred to the coarse grid using appropriate mortar operator.

The above sketched strategy has several advantages. First, all nonlinearities of the problem

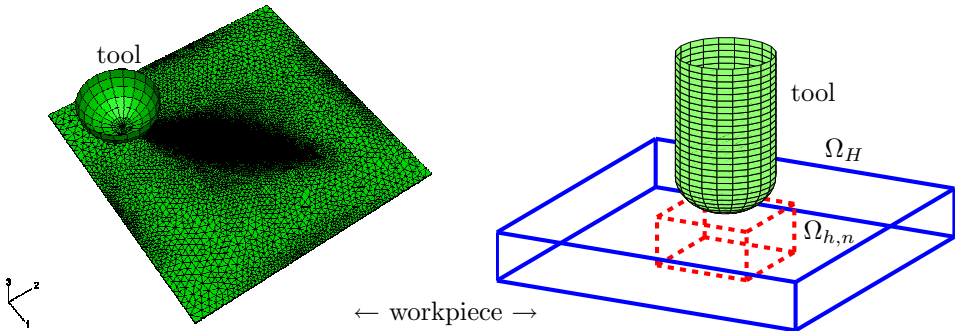

Figure 2: Left: ©IBF, Aachen, Abaqus simulation with adaptive mesh refinement, right: ODDM.

can be separated from the coarse grid. As a result, the stiffness matrix of the linear coarse problem has to be assembled only once which saves a lot of computational time. Second, the fine patch, the plastic zone and the contact interface can be resolved in detail without discretizing the workpiece with a global fine grid, which would lead to high computational cost and complex data transfer caused by remeshing.

The current formulation of the method is limited to small deformations. Such assumption is reasonable since, for example, the deep rolling process can be modelled at a first approximation in the regime of small deformations. Nevertheless, other problems like geometrically nonlinear contact problems for thin structures and velocity-based contact formulations can be considered as well using the developed framework.

The first generalization is related to the dynamic contact of thin-walled 3D bodies including large deformations. For this problem, the contact formulation is presented in the context of implicit structural dynamics. Two different time discretization schemes, the Generalized-α Method [16] and the Generalized Energy-Momentum Method [32], are considered. To end up with an energy conserving framework, an idea by Laursen and Love [33] is picked up who introduce a discrete contact velocity to update the velocity field in a post-processing step. The generalization of this approach to the utilized time integration schemes as well as the incorporation into the primal-dual active set strategy is presented. Finally, an algorithm for a surface oriented shell element based on a 3D formulation with seven parameters, including the thickness stretch of the shell [14], has been suggested. See [25, 24] for further details.

A different type of application for the developed algorithms is velocity-driven problems, i.e., the existing displacement-based contact formulation has been adapted to a velocity-based one [10, 11]. The method has been applied to the ring rolling of external spur gears, which is a rigid-plastic metal forming simulation. The difficulty of the large deformations is tackled in an updated Lagrangian manner.

We now turn to a more detailed presentation of the developed approaches. Our main focus is on the description of the general framework for contact and plasticity as well as on the overlapping domain decomposition approach.

2 Model and problem setting

We assume a relatively simple elasto-plastic behavior of the working piece $\Omega \subset \mathbb{R}^3$ with sufficiently smooth boundary $\partial\Omega$. The chosen flow model is J_2-plasticity with small deformations and isotropic hardening, see, e.g., [42, 3, 23, 47]. This assumption is mainly for ease of presentation, and the method can be extended to more comprehensive models.

The assumption of small deformations allows for an additive decomposition of the symmetric

linear strain tensor $\boldsymbol{\varepsilon} \in \mathbb{R}^{3\times3}$, into an elastic part $\boldsymbol{\varepsilon}^e$ and a plastic part $\boldsymbol{\varepsilon}^p$, $\boldsymbol{\varepsilon}^e = \boldsymbol{\varepsilon} - \boldsymbol{\varepsilon}^p$. The governing equations for the constitutive law are

$$\boldsymbol{\sigma} = \mathbf{C}^{el}\boldsymbol{\varepsilon}^e, \quad \dot{\boldsymbol{\varepsilon}}^p = \lambda \partial_{\boldsymbol{\sigma}} \Phi(\boldsymbol{\sigma}, \alpha) \quad \dot{\alpha} = \lambda; \quad \lambda \geqslant 0, \quad \Phi(\boldsymbol{\sigma}, \alpha) \leqslant 0, \quad \lambda\Phi(\boldsymbol{\sigma}, \alpha) = 0$$

with $\boldsymbol{\sigma} \in \mathbb{R}^{3\times3}$ denoting the actual Cauchy stress tensor and $\lambda \in \mathbb{R}$ the plastic consistency parameter. Further, $\mathbf{C}^{el}$ is the fourth order Hook tensor for the linear elastic material, and $\Phi : \mathbb{R}^{3\times3} \times \mathbb{R} \to \mathbb{R}$ stands for the yield function defined by $\Phi(\boldsymbol{\sigma}, \alpha) = \bar{\boldsymbol{\sigma}} - Y(\alpha)$, where $Y : \mathbb{R} \to \mathbb{R}$ denotes the function of isotropic hardening with the hardening parameter $\alpha \in \mathbb{R}$, and $\bar{\boldsymbol{\sigma}}$ is the equivalent stress. In the simplest case of von Mises stress and linear isotropic hardening, they are given by

$$\bar{\boldsymbol{\sigma}} = \sqrt{3/2\ \mathrm{dev}\,\boldsymbol{\sigma} : \mathrm{dev}\,\boldsymbol{\sigma}}, \quad Y(\alpha) = Y(0) + K\alpha,$$

with a constant $K \geq 0$.

Before the spatial discretization, a time discretization into time intervals $[t_n, t_{n+1}]$, $n = 0, 1, \ldots$ is performed using the implicit Euler scheme. The global equilibrium at the current time step t_{n+1} with the external forces $\boldsymbol{f}^{ext}_{n+1}$ acting on the body then reads

$$f^{int}(\boldsymbol{u}_{n+1}, \boldsymbol{v}) = \int_\Omega \boldsymbol{\sigma}_{n+1}(\boldsymbol{u}_{n+1}) : \boldsymbol{\varepsilon}(\boldsymbol{v}) = \int_\Omega \boldsymbol{f}^{ext}_{n+1}\ \boldsymbol{v} = l^{ext}_{n+1}(\boldsymbol{v}), \quad \boldsymbol{v} \in [H^1_0(\Omega)]^3 \tag{1}$$

The relation $\boldsymbol{\sigma}_{n+1}(\boldsymbol{u}_{n+1})$ is nonlinear, since $\boldsymbol{\sigma}_{n+1}$ is the stress which is projected onto the yield surface. By $H^1_0(\Omega)$, the space of test functions with homogeneous Dirichlet boundary conditions on $\partial\Omega$ is denoted.

The interaction between the tool and the workpiece Ω is modeled as a one-body contact problem with a rigid obstacle. For simplicity, friction is neglected throughout this work, but Tresca as well as Coulomb friction can be incorporated in the algorithms presented here [28]. The part of $\partial\Omega$ which comes potentially into contact with Γ^{tool} is called Γ^{con}.

The contact conditions can be written as (the time index n is omitted):

$$\boldsymbol{u} \cdot \boldsymbol{\nu} - g \leq 0, \quad \sigma_\nu(\boldsymbol{u}) \leq 0; \quad \sigma_\nu(\boldsymbol{u})\,(\boldsymbol{u} \cdot \boldsymbol{\nu} - g) = 0, \quad \boldsymbol{\sigma}_\tau\,(\boldsymbol{u}) = 0, \tag{2}$$

where g is the gap function, $\boldsymbol{\nu}$ is outward unit normal and σ_ν and $\boldsymbol{\sigma}_\tau$ are the normal and the tangential parts of the boundary stresses, respectively [7]. The first condition means that no penetration is allowed, and the second allows only compression but no tension, since we assume that there are no adhesion effects. The third equation is the complementarity condition that means that non-zero contact stresses can only occur if the gap is zero. The last equation means that the stress in tangential direction vanishing since there is no friction.

For simplicity volume forces and other external forces are assumed to be zero except for the contact forces from now on. Then, the equilibrium is given by: Find $\boldsymbol{u} \in [H^1_0(\Omega)]^3$ such that

$$f^{int}(\boldsymbol{u}, \boldsymbol{v}) + \int_{\Gamma^{con}} \boldsymbol{\lambda} \cdot \boldsymbol{v} = 0, \tag{3}$$

for arbitrary test functions $\boldsymbol{v} \in [H^1_0(\Omega)]^3$ and with the internal forces f^{int} depending nonlinearly on $\boldsymbol{u}$. The Lagrange multiplier $\boldsymbol{\lambda} = -\boldsymbol{\sigma}(\boldsymbol{u})\boldsymbol{\nu}$ can be interpreted as the negative contact stress, but is introduced as an additional unknown to enforce the contact conditions.

3 Unified framework for plasticity and contact

In this section we introduce a single mesh finite element method for the solution of (3) and outline the important features of the constructed approximations. Later on, the presented algorithms will be used for the construction of the solver for the fine subdomain.

As mentioned before, the problem incorporates two nonlinearities, namely the elasto-plastic material behavior and the contact interaction. The presented approach allows to consider both

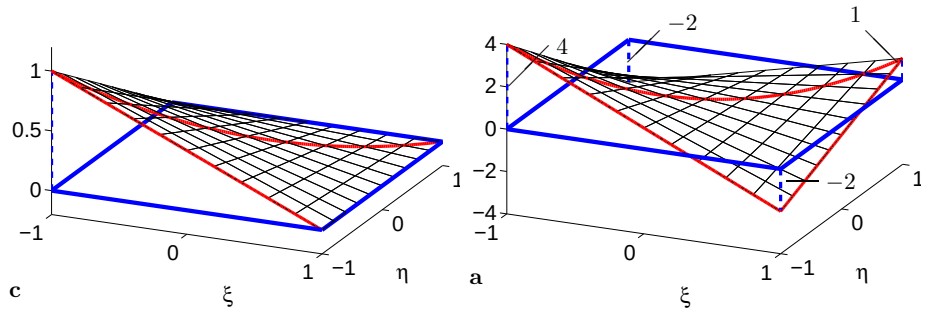

Figure 3: Standard bilinear basis function φ_q (left) and corresponding dual LM ψ_p (right).

of them in a unified way, based on the idea that the primal-dual active set strategy for contact can be interpreted as a semismooth Newton method [1, 26] and can be adapted to nonlinear material behavior, as demonstrated in [10, 11]. This means that both physical and geometrical nonlinearities are handled in the same semi-smooth Newton loop. This is in contrast to standard approaches, where nested iteration cycles are used to deal with contact conditions and nonlinear material behavior.

Let us assume for a moment that no contact interaction is accounted for and, therefore, the problem is just an elasto-plastic problem. We discretize the domain Ω in space using lowest order conforming hexahedral finite elements, leading to the finite-dimensional approximation $\boldsymbol{u}_{h,n+1}$ of the solution $\boldsymbol{u}_{n+1}$. Further, we define the vectors $\boldsymbol{F}^{int}(\boldsymbol{U}_{n+1})$ and $\boldsymbol{F}^{ext}$ as the standard FE assemblies of f^{int} and l^{ext}, where $\boldsymbol{U}_{n+1}$ stands for the vector of nodal values of $\boldsymbol{u}_h$. With this, we can formulate the finite-dimensional version of the equilibrium equation (1):

$$\boldsymbol{F}^{int}(\boldsymbol{U}_{n+1}) - \boldsymbol{F}^{ext} = \boldsymbol{0}.$$

After consistent linearization [43, 42] one gets a global system of linear equations with the tangential stiffness $\mathbf{K}_{n+1}^{(j)}$ in the j-th Newton step.

To handle the nonlinearity of the contact conditions, we use the primal-dual active set strategy combined with dual Lagrange multipliers [46, 29]. The Lagrange multiplier $\boldsymbol{\lambda}$, which is introduced as an additional unknown for the contact stress (see eqrefeq:root), is approximated by

$$\boldsymbol{\lambda}_h = \sum_{p \in \mathbb{S}} \boldsymbol{\Lambda}_p \psi_p \in \mathbb{R}^3$$

with the dual Lagrange multipliers basis functions ψ_p and $\mathbb{S}$ denoting the set of all potential contact nodes on the contact zone Γ^{con}.

We briefly outline the main properties of dual Lagrange multipliers. They are constructed to be biorthogonal with respect to to the standard basis functions φ_i, i.e.:

$$\mathbf{B}_{pq} = \int \psi_p \varphi_q \, d\Gamma = \delta_{pq} \int \varphi_q \, d\Gamma, \quad p, q \in \mathbb{S}. \tag{4}$$

The sketch of a dual basis function ψ_i is presented on Fig. 3 (right), while the corresponding standard bilinear basis function φ_q is shown on Fig. 3 (left). For literature about dual Lagrange multipliers, we refer the reader to [20, 46], and to [4, 2, 5] and the references therein for an overview of the mortar method. See especially [25] and the references therein for the situation when Γ^{con} is two-dimensional and meshed with quadrilaterals.

Using these dual Lagrange multipliers, the algebraic representation of the equilibrium has the form

$$\boldsymbol{F}^{int}(\boldsymbol{U}) + \mathbf{B}\boldsymbol{\Lambda} = \mathbf{0} \tag{5}$$

where the entries of the coupling matrix are defined in (4), and $\boldsymbol{\Lambda}$ contains the nodal values of the Lagrange multipliers. Using an appropriate node numbering and due to the biorthogonality relation (4), $\mathbf{B}$ has the form $\mathbf{B} = (\mathbf{0}\ \mathbf{D})^\top$ with a diagonal matrix $\mathbf{D}$ [11].

Next, the contact conditions (2) have to be discretized. The strong pointwise non-penetration condition is replaced by a weaker integral condition which, due to (4), can be written pointwise in an algebraic representation as

$$U_{\nu,p} = \boldsymbol{N}_p^\top \mathbf{D}_{pp} \boldsymbol{U}_p \leqslant G_p, \qquad p \in \mathbb{S} \tag{6}$$

where $\boldsymbol{U}_p \in \mathbb{R}^3$ stands for the coefficient vector of $\boldsymbol{U}_h$ associated with the vertex p, and G_p is the approximation of the gap function at node p. The normal vector at the vertex p is denoted by $\boldsymbol{N}_p$. The condition that no tension stresses can occur is discretized by $\Lambda_{\nu,p} \geqslant 0$ at each vertex $p \in \mathbb{S}$, where $\Lambda_{\nu,p}$ is defined according to (6) by $\Lambda_{\nu,p} = \boldsymbol{N}_p^\top \mathbf{D}_{pp} \boldsymbol{\Lambda}_p$, $\boldsymbol{\Lambda}_p \in \mathbb{R}^3$. Introducing the tangential part of the Lagrange multiplier $\boldsymbol{\lambda}$ at the vertex $p \in \mathbb{S}$ by $\boldsymbol{\Lambda}_{\tau,p} = \boldsymbol{\Lambda}_p - (\boldsymbol{\Lambda}_p \cdot \boldsymbol{N}_p)\boldsymbol{N}_p$, we can write the continuous contact complimentarity conditions (see (2)) in its discrete algebraic form as

$$U_{\nu,p} \leqslant G_p, \;\; \Lambda_{\nu,p} \geqslant 0, \;\; \Lambda_{\nu,p}(U_{\nu,p} - G_p) = 0, \;\; \boldsymbol{\Lambda}_{\tau,p} = \mathbf{0}, \quad p \in \mathbb{S}. \tag{7}$$

In the next paragraph, we present the algorithm for the complete elasto-plastic contact problem on a single mesh.

The unit tangential vectors to Γ^{con} are given by $\boldsymbol{T}_p^{(\xi)} \perp \boldsymbol{N}_p$ and $\boldsymbol{T}_p^{(\eta)} = \boldsymbol{T}_p^{(\xi)} \times \boldsymbol{N}_p$, and we set $\mathbf{T}_\mathbb{S} = \left[\mathbf{T}_\mathbb{S}^{(\xi)} \; \mathbf{T}_\mathbb{S}^{(\eta)}\right]^T$. It can easily be shown that the system (7) is equivalent to the following nonlinear problem:

$$\boldsymbol{F}^{con} = \begin{bmatrix} \boldsymbol{F}_\nu^{con} \\ \mathbf{T}_\mathbb{S} \, \boldsymbol{\Lambda}_\mathbb{S} \end{bmatrix} = \mathbf{0}$$

with

$$\boldsymbol{F}_\nu^{con}(U_{\nu,p}, \Lambda_{\nu,p})[p] = \Lambda_{\nu,p} - \max\{\Lambda_{\nu,p} + c(U_{\nu,p} - G_p), 0\}, \quad p \in \mathbb{S}. \tag{8}$$

The constant $c > 0$ is a scaling factor between the non-penetration condition and the contact stress condition which is necessary since $\boldsymbol{\lambda}$ and $\boldsymbol{u}$ are of different magnitude.

The function $\boldsymbol{F}_\nu^{con}$ is called a nonlinear complimentarity function (NCP). Formally, it just provides a way to rewrite the contact inequality constraints (7) as a system of nonsmooth equalities (8). Nevertheless, such formalization is rather useful since, first, it allows to consider both nonlinear material behavior and contact using one nonlinear system of equations, such that a semi-smooth Newton method can directly be applied. Second, some freedom exists in the definition of an appropriate NCP function which can be used to construct regularized Newton iterations with improved convergence properties [22].

Using (8), the nonlinear equation system (5) is expanded to:

$$\begin{array}{lcll} \boldsymbol{F}^{int}(\boldsymbol{U}) & + \; \mathbf{B}\boldsymbol{\Lambda} & = & \mathbf{0}, \\ \boldsymbol{F}^{con}(\boldsymbol{U}, \boldsymbol{\Lambda}) & & = & \mathbf{0}. \end{array} \tag{9}$$

The next task is to linearize (9) in a consistent way. Applying the semi-smooth Newton method with iteration index j to (9), the derivatives depend on the value of max-function at the last iteration. For this, we define the set $\mathbb{A} = \mathbb{A}^{(j)}$ of active and the set $\mathbb{I} = \mathbb{I}^{(j)}$ of inactive nodes at the j-th iteration as

$$\mathbb{I}^{(j)} = \{p \in \mathbb{S} : \Lambda_{\nu,p}^{(j)} + c(U_{\nu,p}^{(j)} - G_p) \leqslant 0\}, \quad \mathbb{A}^{(j)} = \{p \in \mathbb{S} : \Lambda_{\nu,p}^{(j)} + c(U_{\nu,p}^{(j)} - G_p) > 0\}. \tag{10}$$

From (8), we can see that

$$\boldsymbol{F}_\nu^{con}[\mathbb{I}] = \boldsymbol{\Lambda}_\mathbb{I}, \quad \boldsymbol{F}_\nu^{con}[\mathbb{A}] = -c(\mathbf{N}_\mathbb{A} \, \boldsymbol{U}_\mathbb{A} - \boldsymbol{G}_\mathbb{A}).$$

Further, we decompose the diagonal matrix $\mathbf{D}$ into $\mathbf{D} = \operatorname{diag}(\mathbf{D}_\mathbb{I}, \mathbf{D}_\mathbb{A})$ according to (10) and introduce the matrix $\mathbf{N}_\mathbb{A} \in \mathbb{R}^{|\mathbb{A}| \times 3|\mathbb{A}|}$, containing the normals $\boldsymbol{N}_p$ and the weighting factors in $\mathbf{D}_{pp}$

associated with the vertices in $\mathbb{A}$. Then, the linearized system at the j-th iteration reads:

$$\begin{bmatrix} \mathbf{K}_{\mathbb{NN}} & \mathbf{K}_{\mathbb{NI}} & \mathbf{K}_{\mathbb{NA}} & \mathbf{0} & \mathbf{0} \\ \mathbf{K}_{\mathbb{IN}} & \mathbf{K}_{\mathbb{II}} & \mathbf{K}_{\mathbb{IA}} & \mathbf{D}_{\mathbb{I}} & \mathbf{0} \\ \mathbf{K}_{\mathbb{AN}} & \mathbf{K}_{\mathbb{AI}} & \mathbf{K}_{\mathbb{AA}} & \mathbf{0} & \mathbf{D}_{\mathbb{A}} \\ \mathbf{0} & \mathbf{0} & \mathbf{0} & \mathbf{I}_{\mathbb{I}} & \mathbf{0} \\ \mathbf{0} & \mathbf{0} & -\mathbf{N}_{\mathbb{A}} & \mathbf{0} & \mathbf{0} \\ \mathbf{0} & \mathbf{0} & \mathbf{0} & \mathbf{0} & \mathbf{T}_{\mathbb{A}} \end{bmatrix}^{(j-1)} \begin{bmatrix} \Delta \boldsymbol{U}_{\mathbb{N}}^{(j)} \\ \Delta \boldsymbol{U}_{\mathbb{I}(j-1)}^{(j)} \\ \Delta \boldsymbol{U}_{\mathbb{A}(j-1)}^{(j)} \\ \Delta \boldsymbol{\Lambda}_{\mathbb{I}(j-1)}^{(j)} \\ \Delta \boldsymbol{\Lambda}_{\mathbb{A}(j-1)}^{(j)} \end{bmatrix} = - \begin{bmatrix} \boldsymbol{F}_{\mathbb{N}}^{int}(\boldsymbol{U}) \\ \boldsymbol{F}_{\mathbb{I}}^{int}(\boldsymbol{U}) + \mathbf{D}_{\mathbb{I}} \boldsymbol{\Lambda}_{\mathbb{I}} \\ \boldsymbol{F}_{\mathbb{A}}^{int}(\boldsymbol{U}) + \mathbf{D}_{\mathbb{A}} \boldsymbol{\Lambda}_{\mathbb{A}} \\ \boldsymbol{\Lambda}_{\mathbb{I}} \\ -(\mathbf{N}_{\mathbb{A}} \, \boldsymbol{U}_{\mathbb{A}} - \boldsymbol{G}_{\mathbb{A}}) \\ \mathbf{T}_{\mathbb{A}} \boldsymbol{\Lambda}_{\mathbb{A}} \end{bmatrix}^{(j-1)} \tag{11}$$

with $\Delta \boldsymbol{U}^{(j)} = \boldsymbol{U}^{(j)} - \boldsymbol{U}^{(j-1)}$ and $\mathbb{N}$ denoting the set of all inner nodes. Here, $\boldsymbol{G}_{\mathbb{A}}$ denotes the vector containing the entries G_p associated with the active vertices $p \in \mathbb{A}$.

It is easy to see that equations $(11)_4$ and $(11)_5$ correspond to the linearization of (8) at the inactive and active nodes, respectively. The contact stresses in $\boldsymbol{\Lambda}$ can easily be computed in a post-process due to the diagonal structure of $\mathbf{D}$:

$$\boldsymbol{\Lambda}^{(j)} = \mathbf{D}^{-1} \left([-[\mathbf{K} \Delta \boldsymbol{U}^{(j)}]_{\mathbb{S}} - \boldsymbol{F}_{\mathbb{S}}^{int}(\boldsymbol{U}^{(j-1)}). \right) \tag{12}$$

With this, a local static condensation of the Lagrange multipliers can be performed to get a reduced system for the incremental displacements $\Delta \boldsymbol{U}$. The resulting system is then:

$$\begin{bmatrix} \mathbf{K}_{\mathbb{NN}} & \mathbf{K}_{\mathbb{NI}} & \mathbf{K}_{\mathbb{NA}} \\ \mathbf{K}_{\mathbb{IN}} & \mathbf{K}_{\mathbb{II}} & \mathbf{K}_{\mathbb{IA}} \\ \mathbf{0} & \mathbf{0} & -\mathbf{N}_{\mathbb{A}} \\ \mathbf{T}_{\mathbb{A}} \mathbf{K}_{\mathbb{AN}} & \mathbf{T}_{\mathbb{A}} \mathbf{K}_{\mathbb{AI}} & \mathbf{T}_{\mathbb{A}} \mathbf{K}_{\mathbb{AA}} \end{bmatrix}^{(j-1)} \begin{bmatrix} \Delta \boldsymbol{U}_{\mathbb{N}}^{(j)} \\ \Delta \boldsymbol{U}_{\mathbb{I}(j-1)}^{(j)} \\ \Delta \boldsymbol{U}_{\mathbb{A}(j-1)}^{(j)} \end{bmatrix} = - \begin{bmatrix} \boldsymbol{F}_{\mathbb{N}}^{int}(\boldsymbol{U}) \\ \boldsymbol{F}_{\mathbb{I}}^{int}(\boldsymbol{U}) \\ \boldsymbol{G}_{\mathbb{A}} - \mathbf{N}_{\mathbb{A}} \boldsymbol{U}_{\mathbb{A}} \\ \mathbf{T}_{\mathbb{A}} \boldsymbol{F}_{\mathbb{A}}^{int}(\boldsymbol{U}) \end{bmatrix}^{(j-1)} . \tag{13}$$

Due to the consistent linearization, superlinear convergence can be expected. Moreover, after elimination of the Lagrange multiplier unknowns, the size of the system remains unchanged during the Newton iterations which makes the implementation of the algorithm more efficient.

4 Dynamic overlapping domain decomposition method

In the previous section, an efficient algorithm for the solution of the nonlinear elasto-plastic contact problem has been described. In order to gain more efficiency, we now combine this method with overlapping domain decomposition technique, which is the topic of this section. For this, we discretize the workpiece Ω with a global coarse mesh of mesh size H and introduce a small overlapping patch near the contact zone with mesh step size $h < H$. Let $\mathbb{T}_H$ and $\mathbb{T}_{h,n}$ be the sets of coarse and fine grid points, respectively. Further, let $\mathbb{T}_{\hat{h}}$ be the set of storage grid points. The latter is not actually involved in the computations but is used to store the plastic history data. Further, let

We denote by $\Gamma_{h,n}$ and $\Gamma_{h,n}^d$ the potential contact zone and the Dirichlet boundary of the fine grid, both depending on time since the fine grid is moving with the tool. By Γ_H, the potential contact zone of the coarse grid is indicated, see Fig. 4.

For convenience, we derive the system of equation for the coupled problem step by step, starting form the simpler case of a linear elastic problem. The following discrete FE spaces are introduced:

$$\mathbb{V}_h \subset [H^1(\Omega_{h,n})]^3, \; \mathbb{V}_H \subset [H^1(\Omega_H)]^3, \; \mathbb{V}_{0h} \subset [H_0^1(\Omega_{h,n})]^3, \; \mathbb{V}_{0H} \subset [H_0^1(\Omega_H)]^3$$

Here, $\mathbb{V}_h$ can be used as a local enrichment of the coarse space $\mathbb{V}_H$, leading to the following two-scale elliptic problem (as considered in [21]): Given an external load density $\boldsymbol{f}^{ext}$, and the symmetric elasticity bilinear form $a(\cdot, \cdot)$, find $\boldsymbol{u} \in \mathbb{V}_{0h} \oplus \mathbb{V}_{0H}$ such that

$$a(\boldsymbol{u}, \boldsymbol{v}) = \int_\Omega \boldsymbol{f}^{ext} \cdot \boldsymbol{v}, \quad \boldsymbol{v} \in \mathbb{V}_{0h} \oplus \mathbb{V}_{0H}.$$

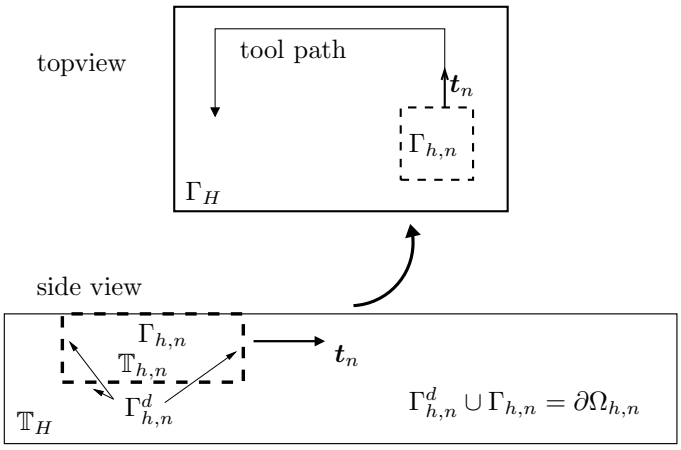

Figure 4: Dynamic ODDM.

After discretization, one arrives at the system

$$\begin{bmatrix} \mathbf{A}_h & \mathbf{A}_{hH} \\ \mathbf{A}_{Hh} & \mathbf{A}_H \end{bmatrix} \begin{bmatrix} \boldsymbol{U}_h \\ \boldsymbol{U}_H \end{bmatrix} = \begin{bmatrix} \boldsymbol{F}_h^{ext} \\ \boldsymbol{F}_H^{ext} \end{bmatrix}, \tag{14}$$

where the Dirichlet boundary conditions on $\partial\Omega_H$ and $\partial\Omega_{h,n}$ are not written explicitly for convenience. The matrices $\mathbf{A}_h$ and $\mathbf{A}_H$ denote the fine and the coarse stiffness matrix, respectively, $\mathbf{A}_{hH}$ is the FE assembly of $a(\boldsymbol{u}, \boldsymbol{v})$ in $\mathbb{V}_{0H} \times \mathbb{V}_{0h}$ and $\mathbf{A}_{Hh}$ the FE assembly of $a(\boldsymbol{u}, \boldsymbol{v})$ in $\mathbb{V}_{0h} \times \mathbb{V}_{0H}$. In [21], the mixed matrices $\mathbf{A}_{hH}$ and $\mathbf{A}_{Hh}$ are set up computing the intersection of elements of the discretization of $\mathbb{V}_h$ and $\mathbb{V}_H$. After this, the resulting block system is solved using iterative technique which relies on the decomposition of the global space into a the direct sum $\in \mathbb{V}_{0h} \oplus \mathbb{V}_{0H}$. In this work, we proceed differently.

First of all, the coupling term $\mathbf{A}_{Hh}$ is neglected completely, since it is assumed that the fine grid correction does not substantially influence the coarse grid solution apart from the contact stresses and the plastic deformation history. Another reason for this simplification is that it guarantees that the matrix in (15) is invertible. As a result, the additive decomposition $\boldsymbol{U} = \boldsymbol{U}_h + \boldsymbol{U}_H$ is unique and the sum $\mathbb{V}_{0h} + \mathbb{V}_{0H}$ does not have to be direct.

Second, the coupling term $\mathbf{A}_{hH}$ is approximated by $\mathbf{A}_h \mathbf{P}_h^{vol}$ with the prolongation operator $\mathbf{P}_h^{vol}$ mapping the coarse solution onto the fine mesh in a consistent way. Thus, the computation of element intersections is not necessary any more, which is especially advantageous for 3D computations with general hexahedral elements. The operator $\mathbf{P}_h^{vol}$ is constructed locally in a stable and robust way by using the same techniques as for the contact coupling operator $\mathbf{P}_h^{con}$. Incorporating these simplifications in (14), one ends up with the block system

$$\begin{bmatrix} \mathbf{A}_h & \mathbf{A}_h \mathbf{P}_h^{vol} \\ \mathbf{0} & \mathbf{A}_H \end{bmatrix} \begin{bmatrix} \boldsymbol{U}_h \\ \boldsymbol{U}_H \end{bmatrix} = \begin{bmatrix} \boldsymbol{F}_h^{ext} \\ \boldsymbol{F}_H^{ext} \end{bmatrix}. \tag{15}$$

The focus of this approach is not the accurate resolution of the underlying elliptic problem, but an efficient numerical scheme which avoids the nonlinearities of contact and plasticity on the global domain. This will be explained in more detail in the next sections, where System (15) is extended by two block rows and columns to account for the contact and plastic effects.

Fine domain subproblem On the fine domain $\Omega_{h,n}$, the full nonlinear elasto-plastic contact problem like in (9) is to be solved, with the only difference that the fine solution $\boldsymbol{U}_h$ is a relative displacement with respect to $\boldsymbol{U}_H$ which is brought up onto $\mathbb{T}_{h,n}$ by means of $\mathbf{P}_h^{vol}$. We assume

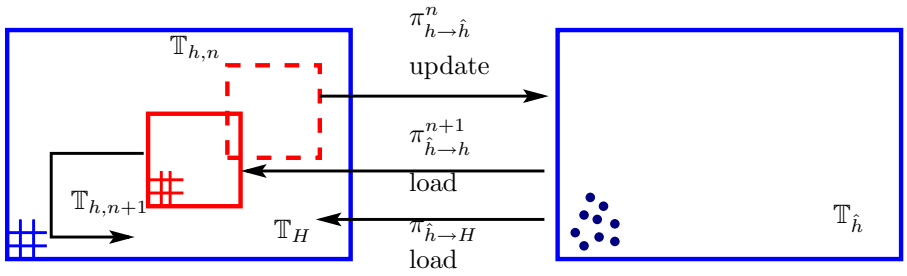

Figure 5: Transfer operators for the plastic data.

that the zone $\Omega_{p,n} \subseteq \Omega_H$ where new plastic deformation takes place is overlapped by the fine computational domain at any time: $\Omega_{p,n} \subseteq \Omega_{h,n}$.

Problem (9) is now reformulated to: Find $\boldsymbol{U}_h, \boldsymbol{\Lambda}_h$ such that $\boldsymbol{U}_h|_{\Gamma^d_{h,n}} = \mathbf{0}$ and

$$\begin{aligned} \boldsymbol{F}_h^{int}(\mathbf{P}_h^{vol}\boldsymbol{U}_H + \boldsymbol{U}_h) + \mathbf{B}\boldsymbol{\Lambda}_h &= \mathbf{0} \qquad (16)\\ \boldsymbol{F}_h^{con}(\mathbf{P}_h^{vol}\boldsymbol{U}_H + \boldsymbol{U}_h, \boldsymbol{\Lambda}_h) &= \mathbf{0} \qquad (17)\end{aligned}$$

The homogeneous Dirichlet conditions on $\Gamma^d_{h,n}$ guarantee the continuity of the composite solution $\boldsymbol{U}_H + \boldsymbol{U}_h$, which is of course a desired feature of this method. Next, we introduce the transfer operators from the coarse to the fine grid and vice versa, see Fig. 5. We denote by $\pi^n_{h\to\hat{h}}$ the transfer operator which maps after each load step t_n the plastic data $(\boldsymbol{\varepsilon}^p_{h,n}, \alpha_{h,n})$ of the fine patch $\Omega^{h,n}$ onto the storage grid $\mathbb{T}_{\hat{h}}$ and updates the data $(\boldsymbol{\varepsilon}^p_{\hat{h},n}, \alpha_{\hat{h},n})$. Conversely, the operator $\pi^{n+1}_{\hat{h}\to h}$ loads the plastic data from the storage grid onto the fine grid in its new position at time t_{n+1}. Finally, the operator $\pi_{\hat{h}\to H}$ loads the plastic data onto the coarse grid Ω_H.

In order to separate the plastic problem from the coarse grid, an auxiliary unknown $\boldsymbol{U}^p_h \in \mathbb{V}_{0h}$ is introduced as the Galerkin projection of the plastic strain increment $\Delta\boldsymbol{\varepsilon}^p_{h,n+1} = \boldsymbol{\varepsilon}^p_{h,n+1} - \pi^{n+1}_{\hat{h}\to h}(\boldsymbol{\varepsilon}^p_{\hat{h},n})$ with respect to the bilinear form $a(\cdot,\cdot)$:

$$\int_{\Omega_{h,n+1}} \boldsymbol{\varepsilon}(\boldsymbol{U}^p_h) : \mathbf{C}^{el} : \boldsymbol{\varepsilon}(\boldsymbol{v}) = \int_{\Omega_{h,n+1}} \Delta\boldsymbol{\varepsilon}^p_{h,n+1} : \mathbf{C}^{el} : \boldsymbol{\varepsilon}(\boldsymbol{v}), \quad \boldsymbol{v} \in \mathbb{V}_{0h}.$$

Note that the plastic dislocations [31] which are captured by the incompatible strain field $\boldsymbol{\varepsilon}^p_h$ are now smoothed out by this projection. In particular, also the residual strains are contained in $\boldsymbol{U}^p_h$. This is the reason why the plastic strain $\boldsymbol{\varepsilon}^p_h$ is stored on the storage mesh $\mathbb{T}_{\hat{h}}$ instead of $\boldsymbol{U}^p_h$. The discrete nonlinear problem (16), (17) is thus supplemented by one additional block row:

$$\begin{aligned} \mathbf{A}_h(\boldsymbol{U}_h - \boldsymbol{U}^p_h) + \mathbf{A}_h\mathbf{P}_h^{vol}\boldsymbol{U}_H + \mathbf{B}\boldsymbol{\Lambda}_h + \boldsymbol{F}^p_{h,n} &= \mathbf{0} \qquad (18)\\ \boldsymbol{F}_h^{con}(\boldsymbol{U}_h + \mathbf{P}_h^{vol}\boldsymbol{U}_H, \boldsymbol{\Lambda}_h) &= \mathbf{0}\\ \boldsymbol{F}_h^{int}(\boldsymbol{U}_h + \mathbf{P}_h^{vol}\boldsymbol{U}_H) - \mathbf{A}_h(\boldsymbol{U}_h - \boldsymbol{U}^p_h) - \mathbf{A}_h\mathbf{P}_h^{vol}\boldsymbol{U}_H - \boldsymbol{F}^p_{h,n} &= \mathbf{0}\end{aligned}$$

where $\boldsymbol{F}^p_{h,n}$ denotes the FE assembly of the fine load correction term

$$l^p_{h,n}(\boldsymbol{v}) = -\int_{\Omega_h} \pi_{\hat{h}\to h}(\boldsymbol{\varepsilon}^p_{\hat{h},n}) : \mathbf{C}^{el} : \boldsymbol{\varepsilon}(\boldsymbol{v}). \qquad (19)$$

On the coarse domain Ω_H, only a linear elastic problem is solved. The discretized contact stresses in $\boldsymbol{\Lambda}_h$ are coupled to the right hand side by means of the mortar operator $\mathbf{P}_H^{con}$ whose construction is explained in the following.

In the discretization of two-body contact problems, mortar methods have frequently been used, see, e.g., [34, 39, 19, 29]. Like sketched in Fig. 6, two domains, denoted by Ω_s (slave) and Ω_m

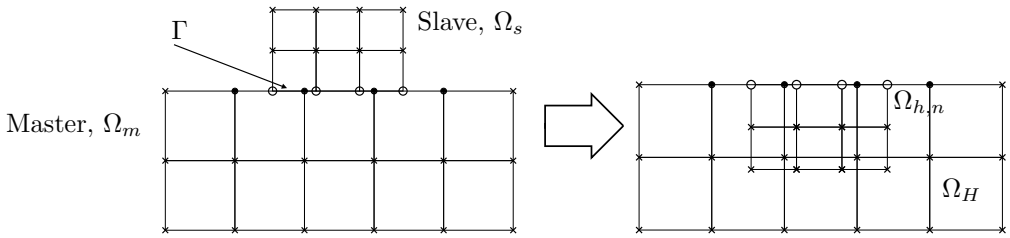

Figure 6: Non-matching meshes: Two-body contact problem (left) and ODDM (right).

(master), come into contact at the interface Γ, where the meshes are in general nonconforming. For our application, we let $\Omega_{h,n}$ play the role of Ω_s, and Ω_H corresponds to the domain Ω_m. The mortar operator $\mathbf{P}_H^{con}$ couples between the dual Lagrange multipliers ψ_p^h of the fine potential contact zone and the coarse standard shape functions on the potential contact zone Γ_H.

Assuming that the contact stress $\boldsymbol{\lambda}$ as well as the plastic strain $\boldsymbol{\varepsilon}^p$ are known from the fine grid computation and stored on the storage grid, we define the load correction term $l_{H,n}^p$ and its standard finite element assembly $\boldsymbol{F}_{H,n}^p$ similarly to (19). With this, we obtain the coarse grid problem, corresponding to the second block row of (15): Find $\boldsymbol{U}_H$ s.t. $\boldsymbol{u}_H|_{\Gamma_H^d} = \mathbf{0}$ and

$$\mathbf{A}_H \boldsymbol{U}_H - \mathbf{P}_H^{vol} \mathbf{A}_h \boldsymbol{U}_h^p + \mathbf{P}_H^{con} \boldsymbol{\Lambda}_h + \boldsymbol{F}_{H,n}^p = \mathbf{0}$$

where $\mathbf{P}_H^{con}\boldsymbol{\Lambda}_h$ is the discretization of the contact forces transfered to the coarse mesh. The operator $\mathbf{P}_H^{vol}$ is a suitable restriction operator constructed similar to $\mathbf{P}_h^{vol}$.

Putting the fine and the coarse sub-systems together, we obtain the coupled nonlinear problem:

$$\boldsymbol{F}(\boldsymbol{X}_h, \boldsymbol{X}_H) = \begin{bmatrix} \mathbf{A}_h(\boldsymbol{U}_h - \boldsymbol{U}_h^p) + \mathbf{A}_h \mathbf{P}_h^{vol} \boldsymbol{U}_H + \mathbf{B}\boldsymbol{\Lambda}_h + \boldsymbol{F}_{h,n}^p \\ \boldsymbol{F}_h^{con}(\boldsymbol{U}_h + \mathbf{P}_h^{vol}\boldsymbol{U}_H, \boldsymbol{\Lambda}_h) \\ \boldsymbol{F}_h^{int}(\boldsymbol{U}_h + \mathbf{P}_h^{vol}\boldsymbol{U}_H) - \mathbf{A}_h(\boldsymbol{U}_h - \boldsymbol{U}_h^p) - \mathbf{A}_h \mathbf{P}_h^{vol}\boldsymbol{U}_H - \boldsymbol{F}_{h,n}^p \\ \mathbf{A}_H \boldsymbol{U}_H - \mathbf{P}_H^{vol}\mathbf{A}_h \boldsymbol{U}_h^p + \mathbf{P}_H^{con}\boldsymbol{\Lambda}_h + \boldsymbol{F}_{H,n}^p \end{bmatrix} = \mathbf{0}. \tag{20}$$

The Jacobi matrix of (20) reads:

$$\mathbf{K} = \frac{d\boldsymbol{F}}{d\boldsymbol{X}} = \left[\begin{array}{c|c} \mathbf{K}_{hh} & \mathbf{K}_{hH} \\ \hline \mathbf{K}_{Hh} & \mathbf{K}_{HH} \end{array}\right] = \left[\begin{array}{ccc|c} \mathbf{A}_h & \mathbf{B} & -\mathbf{A}_h & \mathbf{A}_h\mathbf{P}_h^{vol} \\ \mathbf{N}_h & \mathbf{T}_h & \mathbf{0} & \mathbf{N}_h\mathbf{P}_h^{vol} \\ \mathbf{K}_h^p & \mathbf{0} & \mathbf{A}_h & \mathbf{K}_h^p\mathbf{P}_h^{vol} \\ \hline \mathbf{0} & \mathbf{P}_H^{con} & -\mathbf{P}_H^{vol}\mathbf{A}_h & \mathbf{A}_H \end{array}\right], \tag{21}$$

where

$$\mathbf{N}_h = \frac{\partial \boldsymbol{F}_h^{con}(\boldsymbol{U}, \boldsymbol{\Lambda})}{\partial \boldsymbol{U}}, \quad \mathbf{T}_h = \frac{\partial \boldsymbol{F}_h^{con}(\boldsymbol{U}, \boldsymbol{\Lambda})}{\partial \boldsymbol{\Lambda}}, \quad \mathbf{K}_h^p = \frac{d\boldsymbol{F}_h^{int}(\boldsymbol{U})}{d\boldsymbol{U}} - \mathbf{A}_h$$

and which can be computed according to the Eq. (11). Skipping the block rows and columns 2 and 3 of (21), one would end up again at the matrix of Eq. (15). Finally, in each Newton step j, a 2×2 system with the stiffness matrix (21) has to be solved. This can efficiently be done using a block iterative scheme such as a block Gauss-Seidel method with iteration index k, see [41] and the references therein: Fix j, for $k = 1, \ldots$ solve

$$\mathbf{K}_{hh}^{(j-1)} \Delta \boldsymbol{X}_h^{(j,k)} = -\boldsymbol{F}_h^{(j-1)} - \mathbf{K}_{hH}^{(j-1)} \Delta \boldsymbol{X}_H^{(j,k-1)} \tag{22}$$

$$\mathbf{K}_{HH}^{(j-1)} \Delta \boldsymbol{X}_H^{(j,k)} = -\boldsymbol{F}_H^{(j-1)} - \mathbf{K}_{Hh}^{(j-1)} \Delta \boldsymbol{X}_h^{(j,k)} \tag{23}$$

The fine system (22) can be solved in the condensed form, c.f. Eq. (13). The $\mathbf{K}_{HH}$ block, which correspond to the global linear problem, does not change during the iterations and time steps, such that its LU decomposition can be pre-computed in advance. As a result, only the small $\mathbf{K}_{hh}$ block has to be inverted at each iteration.

Algorithm 1 Inexact Newton Method.

1: **input:** $[\boldsymbol{X}^{(j-1)}, \boldsymbol{F}(\boldsymbol{X}^{(j-1)}), \mathbf{K}(\boldsymbol{X}^{(j-1)}), \eta_j]$
2: **for** $k = 1, \ldots$ **do**
3: $\quad \Delta\boldsymbol{X}^{(j,k)} = \text{ITERATIVE\_SOLVER}(\Delta\boldsymbol{X}^{(j,k-1)}, \mathbf{K}, \boldsymbol{F})$
4: $\quad$ **if** $||\boldsymbol{F}(\boldsymbol{X}^{(j-1)}) + \mathbf{K}(\boldsymbol{X}^{(j-1)})\Delta\boldsymbol{X}^{(j,k))})|| \leqslant \eta_j ||\boldsymbol{F}(\boldsymbol{X}^{(j-1)})||$ **break**
5: **end for**
6: **output:** $\boldsymbol{X}^{(j)} = \boldsymbol{X}^{(j-1)} + \Delta\boldsymbol{X}^{(j,k)}$

Algorithm 2 Complete coupling algorithm.

1: **input:** $[\mathbb{A}^{(0)}, \text{TOL}_{newt}, [\boldsymbol{\varepsilon}^p_{\hat{h},n}, \alpha_{\hat{h},n}]]$
2: Set $j = 1$
3: Assemble the stiffness matrix $\mathbf{K}(\boldsymbol{X}^{(j-1)})$ according to (21) and the right hand side $\boldsymbol{F}(\boldsymbol{X}^{(j-1)})$ according to (20)
4: Compute η_j according to (24) and use Algorithm 1 with the input

$$[\boldsymbol{X}^{(j-1)}, \boldsymbol{F}(\boldsymbol{X}^{(j-1)}), \mathbf{K}(\boldsymbol{X}^{(j-1)}), \eta_j]$$

to compute $\boldsymbol{X}^{(j)}$
5: Update $\mathbb{I}^{(j)}$ and $\mathbb{A}^{(j)}$ using (10)
6: **if** $\|\boldsymbol{F}(\boldsymbol{X}^{(j)})| < \text{TOL}_{newt}$ **goto** 7 **else set** $j = j + 1$ **and goto** 3
7: update $\boldsymbol{\varepsilon}^p_{\hat{h},n+1} = \pi^{n+1}_{h\to\hat{h}}(\boldsymbol{\varepsilon}^p_{h,n+1}, \alpha_{h,n+1})$

A very important issue in combining the Newton method for the nonlinear problem (20) with an iterative linear solver as in (22),(23) is to avoid the so-called oversolving. As illustrated in [18], oversolving means that too many inner iterations are performed during the early Newton steps where the nonlinear function and its local linear model differ much. A possibility to avoid this effect is to control the relative error tolerance of the linear solver by a so-called forcing term η_j (c.f. Alg. 1). There are several possibilities to chose η_j [17, 18], one possibility is

$$\eta_j = \min\left\{\frac{\|\boldsymbol{F}(\boldsymbol{X}^{(j-1)}) - \boldsymbol{F}(\boldsymbol{X}^{(j-2)}) - \mathbf{K}(\boldsymbol{X}^{(j-2)})\Delta\boldsymbol{X}^{(j-1)}\|}{\|\boldsymbol{F}(\boldsymbol{X}^{(j-2)})\|}, 1-\epsilon\right\} \tag{24}$$

with a small number $0 < \epsilon \ll 1$. This criterion reflects the agreement between $\boldsymbol{F}$ and its local linear model at the previous Newton step.

Finally, the complete iterative solution procedure for the load step $t_n \to t_{n+1}$ is summarized in Algorithm 2.

5 Numerical results

In this section we present some numerical results using the presented approaches.

We start with a single domain problem. Fig. 7 shows the comparison of the results obtained by the penalty method and the Lagrange multipliers approach combined with primal-dual active set method. One can observe that quite large penalty parameter is needed in order to obtain an accurate solution comparable with the one obtained using Lagrange multipliers. In Fig. 7 (right), the residual reduction during the iterative solution of the resulting system using a AMG-preconditioned BiCGStab method. The penalty version converges much slower and not as steady as the primal-dual active set method. The reason for this is the deterioration of the condition number of the system due to large values of the penalty parameter ($\rho \sim 10^9$). This provides a strong motivation to use variationally consistent approaches without any "artificial" regularization parameters.

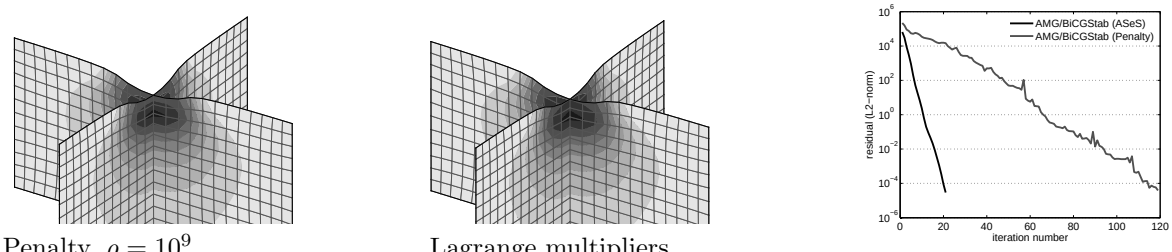

Penalty, $\rho = 10^9$ Lagrange multipliers Convergence history

Figure 7: Penalty vs primal-dual active set method

The next Fig. (5) illustrates the importance of consistent data transfer operators. For this, we show the results of the contact patch test where a constant load can be reproduced by the transfer operator. One can see that in the case of nested meshes on the contact interface, both the simple interpolation approach and the mortar coupling provide the same results. Nevertheless, the situation is rather different in the non-nested case. It is clearly visible that the interpolation approach produces very large errors and does not give correct results even in the case when simple piece-wise constant tractions are applied.

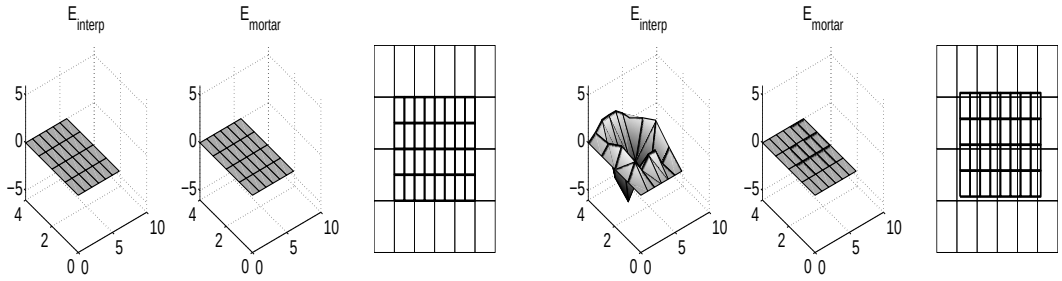

Figure 8: Error of the standard interpolation coupling (E_{interp}) and of the mortar coupling (E_{mortar}) plotted on the coarse grid for $h = 0.5, H = 1.0$.

The next series of figures illustrates the applicability of the overlapping domain decomposition method. Fig. 9 (left) shows the case of a single fine subdomain moving through the working piece along the predefined path. Only the top surface of the working piece is shown, although the complete problem is three-dimensional. Fig. 9 (right) shows remaining displacements $\boldsymbol{U}_h^p$

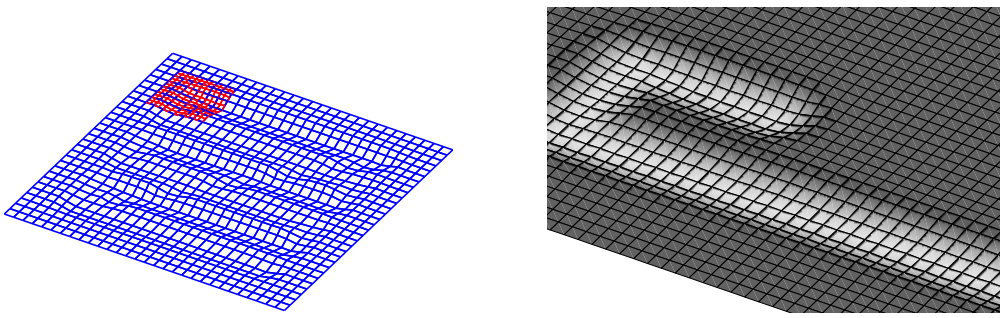

Figure 9: Displacements of fine and coarse grid (left) and remaining displacements on the storage grid (right)

plotted on the storage mesh together with the deformed geometry.

Figure 10 shows examples for the case of 2 or 3 working tools (and 2 or 3 fine sub-domains, respectively). Every working tool and corresponding fine patch may have different geometry, indention depth, mesh parameters, etc. These examples correspond to the case of a deep rolling-like process. Again, the complete problem is three dimensional, and only upper surface is shown on the plots.

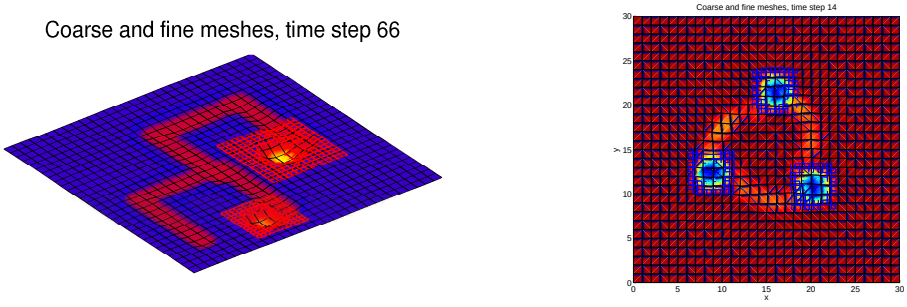

Figure 10: Two and three fine subdomains

Fig. 11 shows the effect of oversolving. The left plot correspond to the case that the linear system at each Newton step is solved with a fixed accuracy of $\epsilon = 10^{-12}$. It is easy to see that a lot of computational time is just wasted since an accurate solution of the linear system does not provide further reduction in the "nonlinear" residual of the Newton's method. In contrast, the modified stopping criterion (24) avoids this drawback, and nearly 50% of the computational time is saved, Fig. 11 (right).

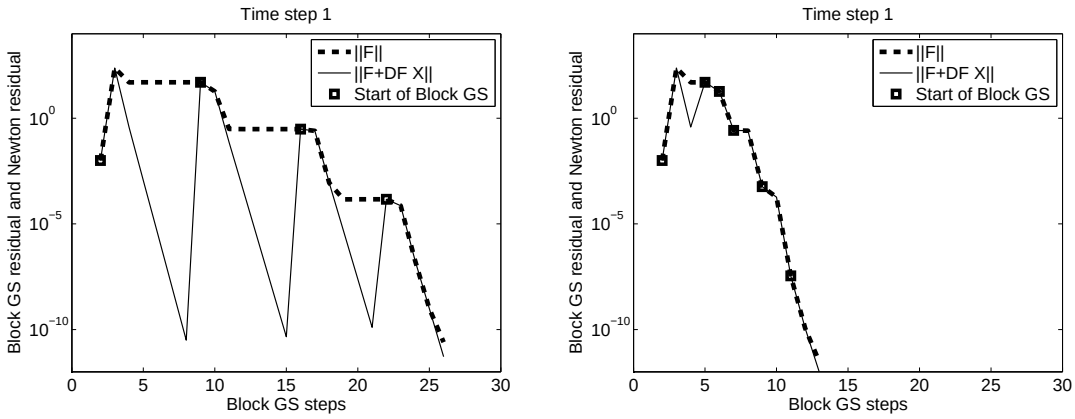

Figure 11: Exact (left) vs inexact (right) block Newton strategy.

Finally, we present some results which illustrate the generalization of the developed algorithms to other problems described. Figure 12 shows the deformed geometry and energy behavior for a thin-walled ball thrown onto an inclined rigid obstacle. The results were obtained using the Generalize Energy-Momentum method and the nonlinear shell formulation for the ball surface. See [25, 24] for further details.

The final example is a velocity-based contact problem, precisely, the ring rolling of an external spur gear. The gear is formed by an external rigid tool and moving internal rigid tool. The material of the forming gear is model using rigid-plastic constitutive law.

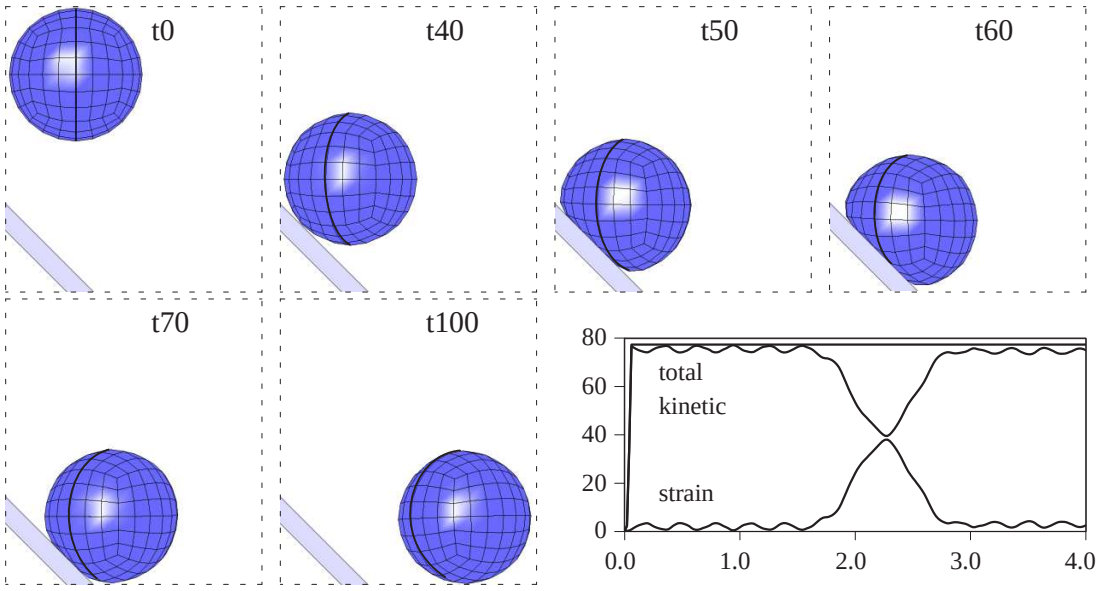

Figure 12: Ball motion and energy dynamics

Figure 13 (left) shows the set up of the simulation. The result after 6000 time steps is shown on the right hand side. We refer to [10, 11] for details.

6 Conclusions

In this work, we described several approaches to construct robust and efficient algorithms for the numerical simulation of incremental metal forming and deep rolling processes. The algorithms are based on a combination of several efficient techniques like the non-smooth inexact Newton method and overlapping domain decomposition. A number of different applications have been considered. Numerical examples illustrate the robustness and the efficiency of the proposed algorithms.

References

[1] P. Alart and A. Curnier. A mixed formulation for frictional contact problems prone to Newton like solution methods. *Comput. Methods Appl. Mech. Engrg.*, 92:353–375, 1991.

[2] F. Ben Belgacem and Y. Renard. Hybrid finite element methods for the Signorini problem. *Mathematics of Computation*, 72(243):1117–1145, 2003.

[3] T. Belytschko, W.K. Liu, and B. Moran. *Nonlinear Finite Elements for Continua and Structures*. John Wiley & Sons, 2000.

[4] F. Ben Belgacem, P. Hild, and P. Laborde. Approximation of the unilateral contact problem by the mortar finite element method. *C. R. Acad. Sci. Paris*, 324:123–127, 1997.

[5] F. Ben Belgacem, P. Hild, and P. Laborde. Extension of the mortar finite element method to a variational inequality modeling unilateral contact. *Mathematical Models and Methods in Applied Sciences*, 9:287–303, 1999.

[6] C. Bernardi, Y. Maday, and A.T. Patera. A new nonconforming approach to domain decomposition: the mortar element method. In H. Brezzi et al., editor, *In: Nonlinear partial differential equations and their applications*, pages 13–51. Paris, 1994.

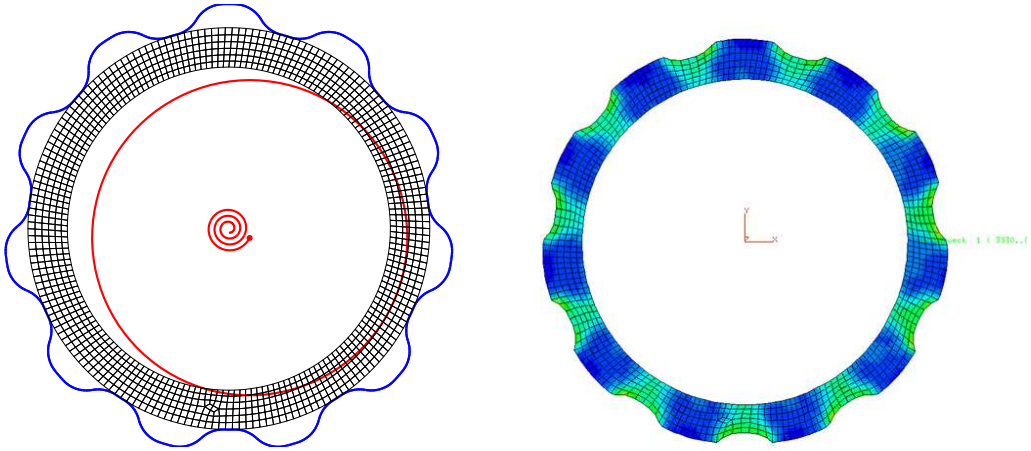

Figure 13: Ring rolling of external spur gear: Initial (left) and final (right) configurations.

[7] S. Brunssen. *Contact analysis and overlapping domain decomposition methods for dynamic and nonlinear problems*. PhD thesis, Universität Stuttgart, 2008.

[8] S. Brunssen, M. Bambach, G. Hirt, and B. Wohlmuth. A primal–dual active set strategy for elastoplastic contact problems in the context of metal forming processes. In R. Owen, E. Onate, and B. Suarez, editors, *Computational Plasticity VIII*, number 2, pages 823–826. Int. Center for Numerical Methods in Engrg., CIMNE, September 2005.

[9] S. Brunßen, C. Hager, B. Wohlmuth, and F. Schmid. Simulation of elastoplastic forming processes using overlapping domain decomposition and inexact Newton methods. In B. Daya Reddy, editor, *Symposium on theoretical, computational and modelling aspects of inelastc media*, volume 11 of *IUTAM Bookseries*, pages 155–164. Springer, 2008.

[10] S. Brunssen, S. Hüeber, and B. Wohlmuth. Contact Dynamics with Lagrange Multipliers. In P. Wriggers and U. Nackenhorst, editors, *Computational Methods in Contact Mechanics*, volume 3 of *IUTAM Bookseries*, pages 17–32. Springer, 2007.

[11] S. Brunssen, F. Schmid, M. Schäfer, and B. Wohlmuth. A fast and robust method for contact problems by combining a primal-dual active set strategy and algebraic multigrid. *Internat. J. Numer. Methods Engrg.*, 69:524–543, 2007.

[12] S. Brunssen and B. Wohlmuth. An elastoplastic coupling algorithm for the simulation of incremental metal forming processes. In E. Onate, M. Papadrakakis, and B. Schrefler, editors, *Computational Methods for Coupled Problems in Science and Engineering II*, pages 133–136. Int. Center for Numerical Methods in Engrg., CIMNE, May 2007.

[13] S. Brunssen and B. Wohlmuth. An overlapping domain decomposition method for the simulation of elastoplastic incremental forming processes. *Internat. J. Numer. Methods Engrg.*, 77:1224–1246, 2009.

[14] N. Büchter and E. Ramm. 3D-extension of nonlinear shell equations based on the enhanced assumed strain concept. In C. Hirsch, editor, *Computational Methods in Applied Sciences*, pages 55–62. Elsevier, 1992.

[15] E. Ceretti, C. Giardini, and A. Attanasio. Sheet incremental forming on CNC machines. In *Proceedings of the SheMet 2003*, pages 49–56, April 2003.

[16] J. Chung and G.M. Hulbert. A time integration algorithm for structural dynamics with improved numerical dissipation: The Generalized-α method. *J. Appl. Mech.*, 60:371–375, 1993.

[17] R.S. Dembo, S.C. Eisenstat, and T. Steighaug. Inexact Newton methods. *SIAM J. Numer. Anal.*, 19:400–408, 1982.

[18] S.C. Eisenstat and H.F. Walker. Choosing the forcing terms in an inexact Newton method. *SIAM J. Sci. Comput.*, 17(1):16–32, 1996.

[19] K.A. Fischer and P. Wriggers. Frictionless 2D contact formulations for finite deformations based on the mortar method. *Comput. Mech.*, 36:226–244, 2005.

[20] B. Flemisch. *Non-matching Triangulations of Curvilinear Interfaces Applied to Electro-Mechanics and Elasto-Acoustics*. PhD thesis, Universität Stuttgart, Shaker Verlag, Aachen, 2007.

[21] R. Glowinski, J. He, A. Lozinski, J. Rappaz, and J. Wagner. Finite element approximations of multi–scale elliptic problems using patches of elements. *Numer. Math.*, 101:663–687, 2005.

[22] C. Hager and B. Wohlmuth. Nonlinear complementarity functions for plasticity problems with frictional contact. *Comput. Methods Appl. Mech. Engrg.*, 198:3411–3427, 2009.

[23] W. Han and B.D. Reddy. *Plasticity, Mathematical Theory and Numerical Analysis*. Springer, 1999.

[24] S. Hartmann, S. Brunßen, E. Ramm, and B. Wohlmuth. A mortar based contact formulation for non-linear dynamic problems using dual Lagrange multipliers. In E. Onate, D.R.J. Owen, and B. Suarez, editors, *Computational Plasticity IX*, 1, pages 133–136. Int.Center for Numerical Methods in Engrg., CIMNE, 2007.

[25] S. Hartmann, S. Brunssen, E. Ramm, and B. Wohlmuth. A primal-dual active set strategy for unilateral non-linear dynamic contact problems of thin-walled structures. *Internat. J. Numer. Methods Engrg.*, 70:883–912, 2007.

[26] M. Hintermüller, K. Ito, and K. Kunisch. The primal-dual active set strategy as a semi–smooth Newton method. *SIAM Journal on Optimization*, 13(3):865–888, 2003.

[27] G. Hirt, M. Bambach, and S. Junk. Modelling of the incremental CNC sheet metal forming process. In *Proceedings of the SheMet 2003*, pages 495–502, April 2003.

[28] S. Hüeber, G. Stadler, and B. Wohlmuth. A primal-dual active set algorithm for three-dimensional contact problems with Coulomb friction. *SIAM J. Sci. Comput.*, 30(2):572–596, 2008.

[29] S. Hüeber and B. Wohlmuth. A primal–dual active set strategy for non–linear multibody contact problems. *Comput. Methods Appl. Mech. Engrg.*, 194:3147–3166, 2005.

[30] F. Klocke and S. Mader. Fundamentals of the deep rolling of compressor blades for turbo aircraft engines. In *Proceedings of the 9th international conference on shot peening*, pages 125–130, Paris, 2005.

[31] E. Kröner. Benefits and shortcomings of the continuous theory of dislocations. *Internat. J. Solids Structures*, 38:1115–1134, 2001.

[32] D. Kuhl and E. Ramm. Generalized energy-momentum method for non-linear adaptive shell dynamics. *Comput. Methods Appl. Mech. Engrg.*, 178:343–366, 1999.

[33] T.A. Laursen and G.R. Love. Improved implicit integrators for transient impact problems - geometric admissibility within the conserving framework. *Internat. J. Numer. Methods Engrg.*, 53:245–274, 2002.

[34] T.W. McDevitt and T.A. Laursen. A mortar finite element formulation for frictional contact problems. *Internat. J. Numer. Methods Engrg.*, 48:1525–1547, 2000.

[35] K. McLoughlin, A. Cognot, and E. Quigley. Dieless manufacturing of sheet metal components with non rigid support. In *Proceedings of the SheMet 2003*, pages 123–130, April 2003.

[36] V. Padmanabhan and T.A. Laursen. Surface smoothing procedure for large deformation contact analysis. *Finite Elem. Anal. Des.*, 37:173–198, 2001.

[37] P. Papadopoulos and R. Taylor. A mixed formulation for the finite element solution of contact problems. *Comput. Methods Appl. Mech. Engrg.*, 94:373–389, 1992.

[38] M.A. Puso and T.A. Laursen. A 3D contact smoothing method using Gregory patches. *Internat. J. Numer. Methods Engrg.*, 54:1161–1194, 2002.

[39] M.A. Puso and T.A. Laursen. A mortar segment–to–segment contact method for large deformation solid mechanics. *Comput. Methods Appl. Mech. Engrg.*, 193:601–629, 2004.

[40] M.A. Puso and T.A. Laursen. A mortar segment-to-segment frictional contact method for large deformations. *Comput. Methods Appl. Mech. Engrg.*, 193:4891–4913, 2004.

[41] Y. Saad. *Iterative Methods for Sparse Linear Systems, 2nd Edition.* SIAM, Philadelphia, 2003.

[42] J.C. Simo and T.J.R. Hughes. *Computational Inelasticity.* Springer, 1998.

[43] J.C. Simo and R.L. Taylor. Consistent tangent operators for rate independent elasto-plasticity. *Comput. Methods Appl. Mech. Engrg.*, 48:101–118, 1985.

[44] M. Stadler and G.A. Holzapfel. Subdivision schemes for smooth contact surfaces of arbitrary mesh topology in 3D. *Internat. J. Numer. Methods Engrg.*, 60:1161–1195, 2004.

[45] B. Wohlmuth. A mortar finite element method using dual spaces for the Lagrange multiplier. *SIAM J. Numer. Anal.*, 38:989–1012, 2000.

[46] B. Wohlmuth. Discretization techniques and iterative solvers based on domain decomposition. *Lecture Notes in Computational Science and Engineering*, 17, 2001. Springer.

[47] P. Wriggers. *Nichtlineare Finite-Element-Methoden.* Springer, 2001.

[48] B. Yang, T.A. Laursen, and X.N. Meng. Two dimensional mortar contact methods for large deformation frictional sliding. *Internat. J. Numer. Methods Engrg.*, 62:1183–1225, 2005.

Stephan Brunßen
Pfaffenwaldring 57
70569 Stuttgart
Germany

Evgeny Savenkov
Pfaffenwaldring 57
70569 Stuttgart
Germany

Barbara Wohlmuth
Pfaffenwaldring 57
70569 Stuttgart
Germany

Erschienene Preprints ab Nummer 2009/001

Komplette Liste: `http://preprints.ians.uni-stuttgart.de`

2009/001 *Sändig, A.-M.:* Nichtlineare Funktionalanalysis mit Anwendungen auf partielle Differentialgleichungen, Vorlesung im Wintersemester 2008/09

2009/002 *Kissling, F., LeFloch, P. G., Rohde, C.:* A kinetic decomposition for singular limits of non-local conservation laws

2009/003 *Haink, J., Haspot, B., Rohde, C.:* Existence of global weak solutions for boundary value problems for compressible fluid models with nonlocal capillary tensor

2009/004 *Flemisch, B., Kaltenbacher, M., Triebenbacher, S., Wohlmuth, B. I.:* The equivalence of standard and mixed finite element methods in applications to elasto-acoustic interaction

2009/005 *Knees, D., Thomas, M., Lalegname, A.:* Birthday Cracks - Proceedings of the Colloquium dedicated to Prof. Dr. Anna-Margarete Sändig on the occasion of her 65th birthday

2009/006 *Melnyk, T., Nakvasiuk, I.A., Wendland, W. L.:* Homogenization of the Signorini boundary-value problem in a thick junction and boundary integral equations for the homogenized problem

2009/007 *Jung, N., Haasdonk, B., Kröner, D.:* Reduced Basis Method for Quadratically Nonlinear Transport Equations

2009/008 *Melnyk, T., Sivak, O.A.:* ASYMPTOTIC ANALYSIS OF A PARABOLIC SEMILINEAR PROBLEM WITH THE NONLINEAR BOUNDARY MULTIPHASE INTERACTIONS IN A PERFORATED DOMAIN

2009/009 *Kissling, F., Rohde, C.:* The Computation of Nonclassical Shock Waves with a Heterogeneous Multiscale Method

2009/010 *Kohr, M., Raja Sekhar, G.P., Wendland, W. L.:* Rigorous estimates for the 2D Oseen-Brinkman transmission problem in terms of the Stokes-Brinkman expansion

2009/011 *Engel, P., Rohde, C.:* Convergence of the Space-Time Expansion Discontinuous Galerkin Method for Scalar Conservation Laws

2009/012 *Rohde, C.:* A local and low-order Navier-Stokes-Korteweg system

2009/013 *Triebenbacher, S., Kaltenbacher, M., Wohlmuth, B. I., Flemisch, B.:* Applications of the Mortar Finite Element Method in Vibroacoustics and Flow Induced Noise Computations

2009/014 *Brunßen, S., Savenko, E., Wohlmuth, B. I.:* Overlapping domain decomposition for incremental sheet metal forming